Crystal structure and distortion of superconducting $Cu_xBi_2Se_3$

Tobias Fröhlich,[1] Zhiwei Wang,[1,2] Mahasweta Bagchi,[1] Anne Stunault,[3] Yoichi Ando,[1] and Markus Braden[1,*]

[1]*II. Physikalisches Institut, Universität zu Köln, Zülpicher Straße 77, D-50937 Köln, Germany*

[2]*Key Laboratory of Advanced Optoelectronic Quantum Architecture and Measurement (MOE), School of Physics, Beijing Institute of Technology, Beijing 10086, People's Republic of China*

[3]*Institut Laue Langevin, 6 Rue Jules Horowitz BP 156, F-38042 Grenoble CEDEX 9, France*

(Received 16 January 2020; revised manuscript received 27 March 2020; accepted 13 April 2020; published 5 May 2020)

The crystal structure of the candidate topological superconductor $Cu_xBi_2Se_3$ was studied by single-crystal neutron diffraction using samples obtained by inserting the Cu dopant electrochemically. Neither structural refinements nor calculated scattering-density maps find a significant occupation of Cu at the intercalation site between the quintuple layers of Bi_2Se_3. Following Bragg reflection intensities as a function of temperature, there is no signature of a structural phase transition between 295 and 2 K. However, the analysis of large sets of Bragg reflections indicates a small structural distortion breaking the rotational axis due to small displacements of the Bi ions.

DOI: 10.1103/PhysRevMaterials.4.054802

I. INTRODUCTION

The discovery of superconductivity in Cu-intercalated Bi_2Se_3 [1] attracts strong interest, because these materials are proposed to be candidates for topological superconductivity. Topological superconductivity is caused by a nontrivial topology in the superconducting wave function and is expected to lead to novel phenomena and quasiparticles, of which Majorana fermions are most prominent. Fu and Berg analyzed the pairing symmetry in $Cu_xBi_2Se_3$ and conclude that the strong spin-orbit coupling in doped Bi_2Se_3 can result in odd-parity superconductivity with such nontrivial topology [2]. The spin-orbit coupling circumvents a strict separation in singlet and triplet pairing, and the spin-orbit-coupled internal degree of freedom takes a triplet. Besides through Cu intercalation, Bi_2Se_3 exhibits superconductivity also for Sr [3,4] or Nb [5] insertion. Support for unconventional superconductivity with spin-triplet-like pairing is detected in temperature-dependent NMR Knight shift experiments, which find only a small change below T_c in the electronic spin susceptibility for most directions of the magnetic field parallel to the layers [6]. This experiment also observes a twofold axis of the Knight shift in the superconducting state, which indicates that the rotational threefold symmetry is broken below T_c [6]. The superconducting transition can thus be associated with nematicity. In the meantime, there is strong support that the superconducting state in all three doped Bi_2Se_3 systems exhibits a lower symmetry [7]. In this nematic superconductivity the threefold rotation axis of the parent material is broken most likely by the anisotropy of the gap amplitude (not only the phase) [7]. Critical magnetic fields exhibit a huge in-plane anisotropy following only a twofold axis [8]. Also, the magnetization, resistivity, and magnetoresistance exhibit twofold symmetry leading to the conclusion that the nematicity is essential for the superconducting phase in doped Bi_2Se_3 [9–13].

An improvement of the sample preparation by electrochemical intercalation and by an annealing step considerably raised the shielding fraction in $Cu_xBi_2Se_3$ [15]. These improved samples exhibit a well-defined anomaly in the specific heat that documents the bulk nature of the superconductivity. Superconductivity occurs in a broad doping range of $0.1 \leqslant x \leqslant 0.5$ and the transition temperature varies less sharply with doping than the shielding fraction [15,16]. Furthermore, the charge carrier density does not follow the amount of doping but stays nearly constant at a rather low value of about 10^{20} cm^{-3} [15,16]. So far, the three different insertions to induce superconductivity in Bi_2Se_3 seem to result in essentially the same physical properties, but the Sr and Nb samples are less air-sensitive and superconducting crystals can be grown from the melt.

The parent compound Bi_2Se_3 crystallizes in the rhombohedral space group $R\bar{3}m$ and the structure consists of quintuple layers of Bi_2Se_3 that are bonded perpendicular to the layers only through the weak van der Waals interaction; see Fig. 1 [17]. In spite of the enormous impact of these candidate topological superconductors, there is little knowledge about the crystal structure in the doped materials. Hor *et al.* deduced from an increase in the c lattice parameter that Cu would occupy an intercalation position in the van der Waals gap between two quintuple layers, at position $3b$ $(0, 0, 1/2)$, see Fig. 1(b) [1], but scanning tunnel microscopy, angle-resolved photoemission spectroscopy, and *ab initio* density functional theory proposed other positions—intercalating and interstitial ones—for the dopant [14]. Li *et al.* report a structural analysis of $Sr_xBi_2Se_3$ by high-resolution transmission electron microscopy and DFT calculations concluding that the Sr dopant is not occupying the intercalation position [18]. In addition,

*braden@ph2.uni-koeln.de

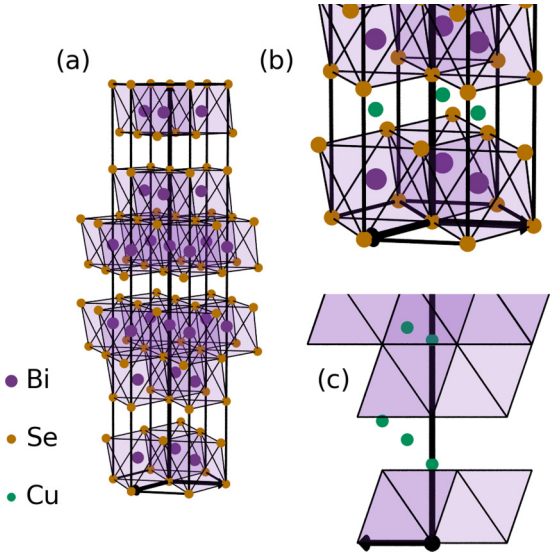

FIG. 1. (a) Crystal structure of Bi_2Se_3 showing the quintuple layers of Bi_2Se_3 separated by the van der Waals gaps. (b) Proposed crystal structure of Cu-doped Bi_2Se_3 with Cu atoms intercalated between the quintuple layers at $(0, 0, 1/2)$ as proposed in Ref. [1]. The Cu sites are expected to be not fully occupied but to depend on the Cu content x. (c) Possible positions for the Cu atoms Cu(i) to Cu(v) according to Ref. [14].

a small structural distortion in the $Sr_xBi_2Se_3$ lattice of about 0.02% was deduced from a high-resolution x-ray study of d values at ambient temperature [19].

Here we report on neutron diffraction studies on superconducting $Cu_xBi_2Se_3$ crystals at room temperature, as well as at temperatures slightly above and below the superconducting transition. Cu-doped Bi_2Se_3 is the prototype compound of this family of unconventional superconductors and such samples are used in various experiments including those documenting the nematic character for the first time. Therefore, we consider it most important to also clarify the crystal structure and the position of the dopant for this material. We cannot detect Cu occupation at any of the proposed intercalation and interstitial sites, and there is no indication of a structural phase transition between room temperature and 2 K. However, structural refinements with large data sets improve when the symmetry is lowered to monoclinic.

II. EXPERIMENTAL

Bi_2Se_3 single crystals were grown from a stoichiometric melt. Pieces of the single crystals were electrochemically doped with Cu using a saturated solution of CuI in CH_3CN. Typical stoichiometries for superconducting $Cu_xBi_2Se_3$ lie in the range $0.12 \leqslant x \leqslant 0.6$, and shielding fractions of up to 50% can be achieved by this technique but the large crystals required for the neutron diffraction experiment yield lower values. Details of the growth process can be found in Ref. [16].

The large samples used for neutron diffraction experiments are shown in Fig. 2. The Cu-doped samples are sensitive to air; therefore, for storage and transport they need to be sealed in glass tubes. They were cleaved and cut to exhibit a

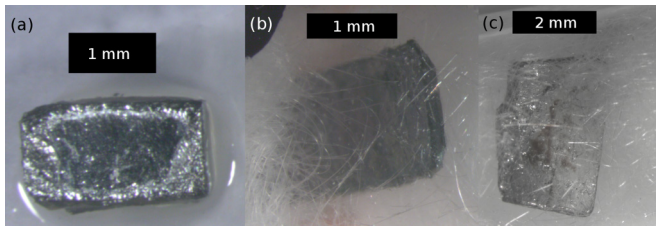

FIG. 2. $Cu_xBi_2Se_3$ samples for neutron diffraction. (a) S1, (b) S2, (c) S3. Since the samples are air sensitive, the photos of the last two samples were taken with the samples sealed in glass tubes and mechanically protected by quartz wool.

platelike shape before the intercalation step and the direction of smallest extension is the c direction of the hexagonal cell. Sample S1 exhibits a Cu amount of $x = 0.30(1)$ ($T_c = 3.1$ K), for sample S2 it amounts to $x = 0.33(1)$ ($T_c = 3.6$ K), and for sample S3 to $x = 0.31(1)$ ($T_c = 3.4$ K). Throughout the paper numbers in parentheses give the error bars of the last digits. Superconducting transition temperatures and shielding fractions were measured in a SQUID magnetometer and the results are shown in Fig. 3. The Cu concentration can be determined by weighting the crystals during the intercalation step but thus only corresponds to the average over the entire crystal.

Single-crystal neutron diffraction was carried out with the three $Cu_xBi_2Se_3$ crystals on the single-crystal neutron diffractometer D9 [20] at the Institut Laue Langevin using a wavelength of 0.84 Å. The sample S1 was measured at a temperature of 300 K, with a pinhole of 5 mm diameter and at the temperatures of 1.9 K and 4.4 K with a pinhole of 6 mm (see Table I). During the data collection at 300 K, a slight misalignment of the pinhole was detected that however turned out insignificant for the data quality. At 1.9 K and 4.4 K, most of the reflections were collected with exposure times between 3 s and 6 s per point in a combined ω-$n\theta$ scan with n between 0 and 2 [20]; at 300 K exposure times amounted to between

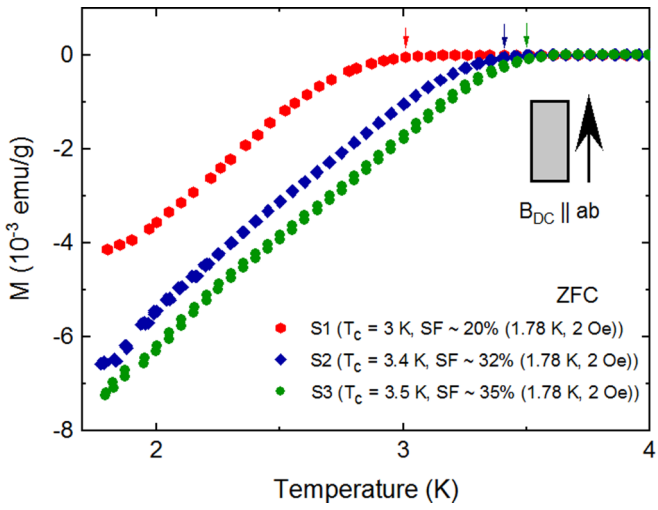

FIG. 3. Zero-field cooled magnetization curves measured with the three single crystals used in the neutron diffraction experiments. The magnetic field of 0.2 mT was applied along the planes. Shielding fractions (SFs) are given in the legend for $T = 1.78$ K.

TABLE I. Number of reflections recorded with the two samples at different temperatures; unique reflections refer to the number of independent reflections after merging in the corresponding space group, and observed reflections exhibit an intensity to error ratio $\frac{I}{\sigma(I)} > 3$.

	Sample S1			Sample S3	
T (K)	300	4.4	1.9	300	2
Number total	530	651	592	640	860
Unique $R\bar{3}m$	157	203	182	137	179
Observed $R\bar{3}m$	124	178	157	557	745
Unique $C2/m$	515	636	577	129	167
Observed $C2/m$	358	428	439	459	632

5 s and 8 s. With sample S2 only temperature-dependent measurements of Bragg intensities were performed. Also with the other two samples Bragg intensities were measured as function of temperature in order to search for a structural phase transition. For sample S3, the optimum pinhole of 7 mm diameter was determined by Renninger scans. At 300 K, most of the reflections were collected with exposure times between 3 s and 5 s per data point, and at 2 K with times between 2 s and 7 s.

The intensity data were absorption corrected using the program DATAP [20]. For sample S1, the orientation was exactly known, and a box geometry with a length of 2.82 mm, a width of 1.55 mm, and a thickness of 0.73 mm was applied. The length and width was determined optically, and the thickness was calculated via the mass of 25.23 mg assuming a density of 7.90 g/cm^3 (where the Cu doping with $x = 0.30$ is taken into account). Sample S3 exhibits a more irregular platelike shape and the area was determined optically to amount to 8.54 mm^2. Via the mass of 46.22 mg and the density, the thickness of 0.69 mm was determined.

III. RESULTS AND DISCUSSION

A. Vacancies and possible Cu positions

First refinements of the crystal structure were performed in space group $R\bar{3}m$ that is reported for the parent compound and that allows for various possible Cu positions. Rhombohedral crystals in general can exhibit two twins corresponding to obverse and reverse setting. The refinements of these twinning fractions for sample S1 yield −0.99(1.23)% at 1.9 K, −0.02(1.65)% at 4.4 K, and 0.46(23)% at 300 K for the reverse setting. The corresponding refinements for sample S3 yield fractions 0.39(1.30)% at 2 K and −0.82(1.99)% at 300 K for the reverse setting. Thus, the samples do not exhibit obverse/reverse twinning.

Se vacancies are supposed to play an important role for transport properties in pure Bi_2Se_3. Therefore, the occupation of the two Se sites were refined. For sample S1 at a temperature of 1.9 K, 4.4 K, and 300 K, the occupation of the Se2 site is 1.011(12), 0.995(16), and 1.002(16), respectively, and the occupation of the Se3 site is 0.999(11), 0.998(14), and 0.985(16), respectively. For sample S3 at 2 K and 300 K, the occupation of the Se2 site is 1.008(10) and 1.003(15), respectively, and the occupation of the Se3 site is 0.989(10) and 1.001(14), respectively. These values are consistent with full occupation. Thus, no Se vacancies could be detected by neutron diffraction.

These refinements not only exclude Se vacancies but also a significant amount of Bi vacancies. We estimate a possible substitution of Bi through Cu by their different neutron scattering lengths: $b_{Cu} = 7.718$ fm and $b_{Bi} = 8.532$ fm [21]. Even though the actual compositions of the crystals are essentially $Cu_xBi_2Se_3$, if we hypothesize a composition $Cu_xBi_{2-x}Se_3$ and apply identical atomic displacement parameters to the Cu and Bi ions, we obtain for sample S1 a Cu substitution of 4(9), −3(12), and −7(13) % at 1.9, 4.4, and 300 K, respectively, and for sample S3 a Cu substitution of −3(8) and 2(11) % at 2 and 300 K, respectively. Note that the precision is rather poor due to the small difference between the scattering lengths of Bi and Cu.

Cu intercalation in the van der Waals gap is expected to enhance the thickness of the van der Waals gap and thus to cause an increase of the c lattice parameter. For pristine Bi_2Se_3, the lattice constants $c = 28.636(20)$ Å [17], 28.615(2) Å [22], and 28.666(1) Å [1] were reported, and for $Cu_{0.12}Bi_2Se_3$, the parameter increases to 28.736(1) Å [1]. LeBail refinements of $(0\,0\,l)$ scans performed on a D5000 x-ray diffractometer with our single crystals yield a lattice constant $c = 28.5990(8)$ Å for undoped Bi_2Se_3 and 28.683(2) Å for $Cu_{0.3}Bi_2Se_3$, confirming the increased lattice constant c due to the insertion of Cu, $\Delta c = 0.084$ Å $\sim 2.9 \times 10^{-3} c$.

The occupation of the most obvious intercalation position at $3b$ $(0, 0, 1/2)$ was examined with the five data sets obtained on two distinct samples by comparing refinements with full occupation, with partial occupation, and without any Cu at this position. For the Cu atom, the displacement parameter was fixed to isotropic $U = 0.005$ Å^2 for the high temperature 300 K respectively $U = 0.0025$ Å^2 for the low temperatures 1.9 K, 2 K, and 4.4 K. The results are shown in Table IV in the Appendix. The five data sets consistently exclude a significant presence of Cu at this position. By combining scanning tunnel microscopy, angle-resolved photoemission spectroscopy, and *ab initio* density functional theory, Wang *et al.* conclude that the most probable sites for the Cu atoms are two interstitial sites within the quintuple layers and three intercalated sites between the quintuple layers [14]. From the caption of Fig. 4 in Ref. [14], it is possible to reconstruct these coordinates. Using the structural parameters from Ref. [17], one gets the following positions: The interstitial atom Cu(i) is located at the position $6c$ $(1/3, 2/3, 0.36127(34))$, and the other interstitial position Cu(ii) is $6c$ $(0, 0, 0.34032(33))$. The coordinates of the three intercalated atoms are $6c$ $(0, 0, 0.1321(15))$ for Cu(iii), $6c$ $(2/3, 1/3, 0.2047(15))$ for Cu(iv), and $6c$ $(1/3, 2/3, 0.1733(15))$ for Cu(v). Other possibilities can be found in Refs. [23] and [18]. All positions proposed in Ref. [14] are tested via structural refinements. A significant occupation was detected in none of these positions; see Table II.

Symmetrized Fourier maps were calculated for the refined models in space group $R\bar{3}m$ for sample S1 at 1.9 K and for sample S3 at 2 K, see Fig. 7 in the Appendix, using the software JANA2006 [24]. The maps show the nuclear scattering density within the unit cell. If an atom is missing in the refinement, there should be an additional peak at this

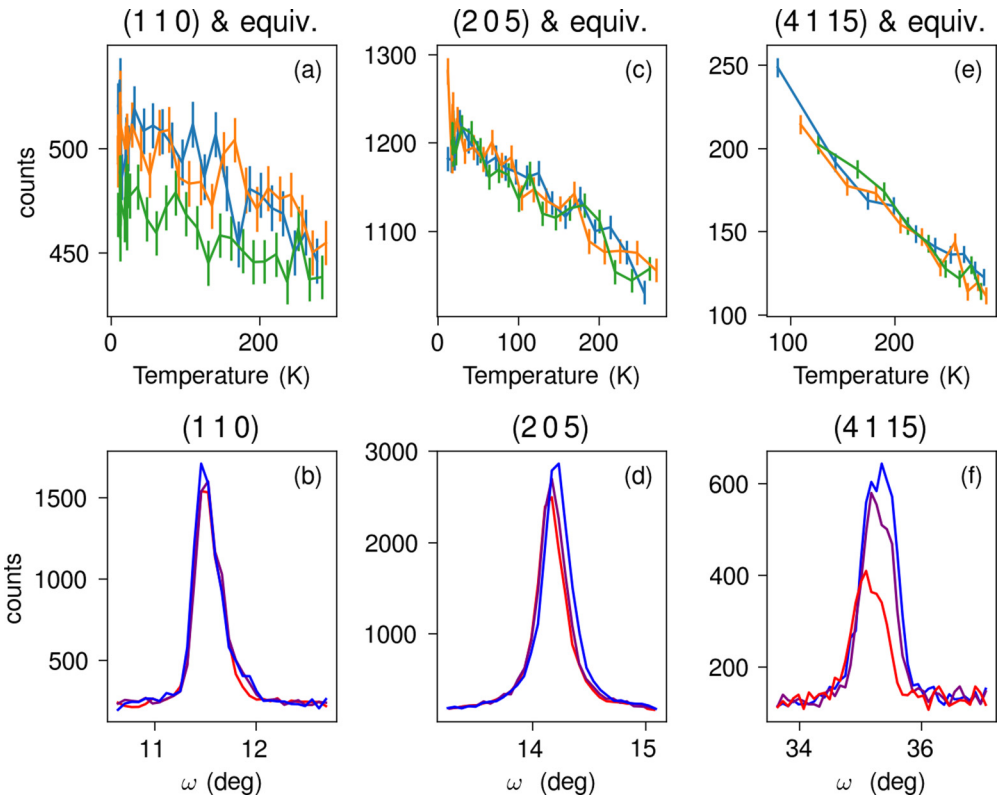

FIG. 4. The upper panels show the temperature dependence of the integrated intensities for three set of equivalent reflections in $R\bar{3}m$: panel (a) (1 1 0), (−1 2 0), and (−2 1 0); panel (b) (2 0 5), (−2 2 5), and (0 −2 5); panel (c) (4 1 15), (1 −5 15), and (−5 4 15). The lower panels show rocking-scan profiles for three different temperatures (the highest temperature in red, the middle in violet, and the lowest in blue). In panel (a) the (1 1 0) is shown at 277, 156, and 9 K; in panel (b) (2 0 5) at 255, 158, and 12 K; in panel (c) (4 1 15) at 284, 143, and 88 K.

position. All atoms of Bi_2Se_3 are clearly visible but no other features appear in the Fourier maps. Shallow peaks like the one at $(1/3, 2/3, 0.025)$ appearing vertically displaced from occupied positions might point to some occupational mixing or insufficient treatment of the atomic displacements. The Fourier maps thus do not indicate the location of the extra Cu ions, and in particular they confirm the absence of a significant amount of Cu at $(0, 0, 1/2)$.

With the precise c lattice parameters determined by our x-ray diffraction experiment and with the structural parameters of Ref. [22] we can compare the width of the van der Waals gap, which amounts to 2.532(4) Å for the parent compound. For the doped compound, we use the average of the z parameter of Se3 determined at 300 K and obtain 2.565(2) Å. The enhancement of the c lattice parameter is thus realized by an increase of the van der Waals gap giving support to the idea that Cu ions are inserted in this gap.

TABLE II. Occupancies (given in percent of full occupation) of the possible Cu positions (i) to (v) that are all located at a Wyckoff position 6*c* from refinements in space group $R\bar{3}m$. There is no significant deviation from zero. Each value was determined by a separate refinement without considering the other Cu positions.

		Cu(i)	Cu(ii)	Cu(iii)	Cu(iv)	Cu(v)
S1	1.9 K	0.4(4)	0.1(4)	0.6(4)	0.4(4)	−0.37(33)
	4.4 K	0.3(5)	0.5(5)	0.2(5)	−0.2(5)	−0.1(4)
	300 K	0.4(5)	0.3(5)	0.4(5)	0.2(5)	0.0(4)
S3	2 K	0.7(4)	0.71(33)	0.58(34)	0.44(34)	−0.43(29)
	300 K	0.6(5)	0.5(5)	0.8(5)	0.6(5)	−0.2(4)

It is thus not possible to detect the position of the inserted Cu with our comprehensive diffraction experiments. At the initially proposed intercalation position and at Cu (v) no Cu can be detected at all, and also the other positions Cu (i) to (iv), see Table II, only yield a total contribution of 0.036(10) [25] for x in the formula $Cu_xBi_2Se_3$ while $x \sim 0.3$ is expected. We must conclude that the Cu atoms do not occupy a well-defined position in $Cu_xBi_2Se_3$, which otherwise would have been detected in the Fourier maps. Instead there must be some positional smearing, which results in very large atomic displacement parameters impairing the detection of the dopant by diffraction. Part of this positional smearing can stem from the separation of superconducting and nonsuperconducting regions that should differ in their Cu content in the distribution of the dopants in the lattice. The ill-defined dopant position can furthermore be the consequence of clustering.

B. Structural phase transition and monoclinic distortion

If a structural phase transition occurs between room and low temperature, one expects some anomalies in the temperature dependence of fundamental Bragg peaks as well. The intensities of three different reflections and their equivalents in space group $R\bar{3}m$ were followed upon cooling; see Fig. 4. The

TABLE III. Positional parameters of the refinements in space groups $R\bar{3}m$ and $C2/m$. Both structures are described here with respect to the hexagonal axes. In both structures Se2 is located at the origin (Wyckoff position 3*a* 0, 0, 0 and 2*a* 0, 0, 0, respectively). The lattice parameters amount to $a = b = 4.143(5)$ Å [17] and $c = 28.683(2)$ Å at 300 K. The c lattice constant was determined by a single-crystal x-ray $(0\,0\,l)$ scan.

			$R\bar{3}m$		$C2/m$	
			Bi1 6c	Se3 6c	Bi1 4i	Se3 4i
S1	1.9 K	x	0	0	−0.0095(5)	−0.0010(9)
		y	0	0	−0.0048(3)	−0.0005(4)
		z	0.40068(4)	0.21098(5)	0.40069(3)	0.21092(3)
	4.4 K	x	0	0	0.0088(7)	0.0035(11)
		y	0	0	0.0044(4)	0.0017(5)
		z	0.40064(6)	0.21076(6)	0.40064(4)	0.21072(4)
	300 K	x	0	0	−0.0103(11)	−0.0021(15)
		y	0	0	−0.0052(5)	−0.0010(7)
		z	0.40061(7)	0.21126(7)	0.40060(5)	0.21121(5)
			$R\bar{3}m$		$C2/m$	
			Bi1	Se3	Bi1	Se3
S3	2 K	x	0	0	−0.0078(3)	−0.0001(5)
		y	0	0	−0.00392(17)	−0.0001(2)
		z	0.40067(4)	0.21112(4)	0.40070(2)	0.21113(2)
	300 K	x	0	0	−0.0120(7)	−0.0009(9)
		y	0	0	−0.0060(3)	−0.0004(4)
		z	0.40070(7)	0.21150(7)	0.40078(4)	0.21148(4)

integrated intensities of most equivalent reflections agree even at low temperature, and there is no anomaly visible in the temperature dependencies of the integrated intensities, which reflect the smaller atomic displacement parameters at low temperature. That there is an enhanced temperature dependence in the reflections (4 1 15) and equivalent ones most likely arises from the different temperature dependencies of the quintuple layers and the van der Waals gaps, but again there is no evidence for a structural phase transition. Also the width of the reflections do not yield any indication for structural phase transition, as the peak profiles that are shown for three reflections in the lower panels of Fig. 4 do not change. These temperature-dependent data were taken with ω scans and a two-dimensional detector resulting in three-dimensional data sets for each Bragg peak at each temperature. We have numerically analyzed the resemblance of these three-dimensional data taken at different temperatures for an individual Bragg peak; see Fig. 6 in the Appendix. This procedure would also detect some anomaly in the mosaic spread due to twinning, but there is no indication for any anomaly in this resemblance analysis. The absence of a structural phase transition agrees with specific-heat measurements indicating a smooth temperature dependence for Sr-doped [10,27] and for Nb-doped [9] Bi_2Se_3.

Breaking of translation symmetry can give rise to superstructure reflections that are forbidden in space group $R\bar{3}m$ and break the general selection rule $-h + k + l = 3n$ [26]. 152 such forbidden reflections were collected at 300 K and 167 at 1.9 K with sample S1. If these reflections are absent, it

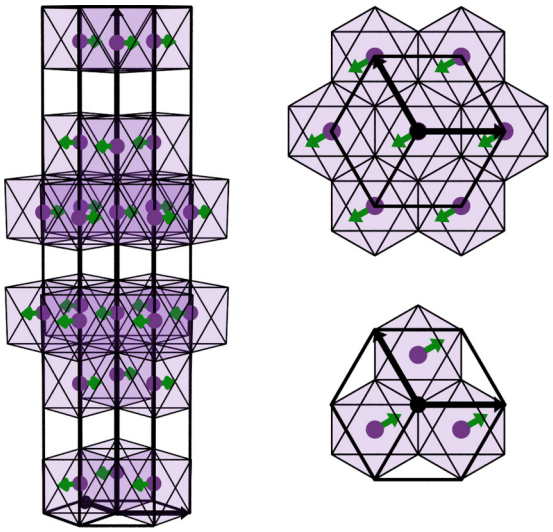

FIG. 5. Left: Distorted crystal structure of $Cu_xBi_2Se_3$ as described in space group $C2/m$. The displacement of the Bi positions of the refinements in $C2/m$ compared to the positions in $R\bar{3}m$ are displayed by arrows. The arrows are 50 times as large as the actual distortions. Right: Two neighboring quintuple layers (viewed along the negative c axis). The displacements are within the monoclinic a, c plane, the mirror plane of $C2/m$.

is expected that ∼68% of the experimental values lie within one standard deviation away from 0. More specifically, the quotient $\frac{I}{\sigma(I)}$ of the intensity divided by its error should exhibit a Gauss distribution with mean value 0 and standard deviation 1. For a few forbidden reflections, a neighboring strong Bragg reflection induces significant intensity, but inspection of the three-dimensional data shows an off-centering and thus a contamination of neighboring Bragg peaks due to the long c axis. After excluding such contaminated reflections the entity of the normalized forbidden intensities exhibits the expected Gauss distribution centered at zero with width 1; therefore we can exclude a significant breaking of the translational symmetry in $Cu_xBi_2Se_3$. The same conclusion was also drawn for Sr-doped Bi_2Se_3 [13].

However, the symmetry can be lower than $R\bar{3}m$ and keep the full translation symmetry, which means that the structural distortion is described by an irreducible representation at the Γ point of the Brillouin zone [28]. There are only two isotropy subgroups of $R\bar{3}m$ that are centrosymmetric and break the threefold rotation axis, $C2/m$ and $P\bar{1}$ [28], and these two only differ in the image of the multidimensional order parameter. Therefore, we may restrict the analysis to the simpler one, $C2/m$, but need to take twinning into account. The monoclinic lattice results from the rhombohedral one by $a' = -2/3a - 1/3b + 2/3c$, $b' = -b$, and $c' = 2/3a + 1/3b + 1/3c$ without a shift of the origin. Note that the primitive lattices are identical for $R\bar{3}m$ and $C2/m$ and there no additional selection rules.

In space group $C2/m$, as in $R\bar{3}m$, there are also three inequivalent sites, Bi1, Se2, and Se3, and compared to the high-symmetry refinement, there are only two additional position parameters, an in-plane displacement for Bi1 and for Se3. For the description of the atomic displacement parameters we keep the constraints from space group $R\bar{3}m$: $U_{11} = U_{22}$,

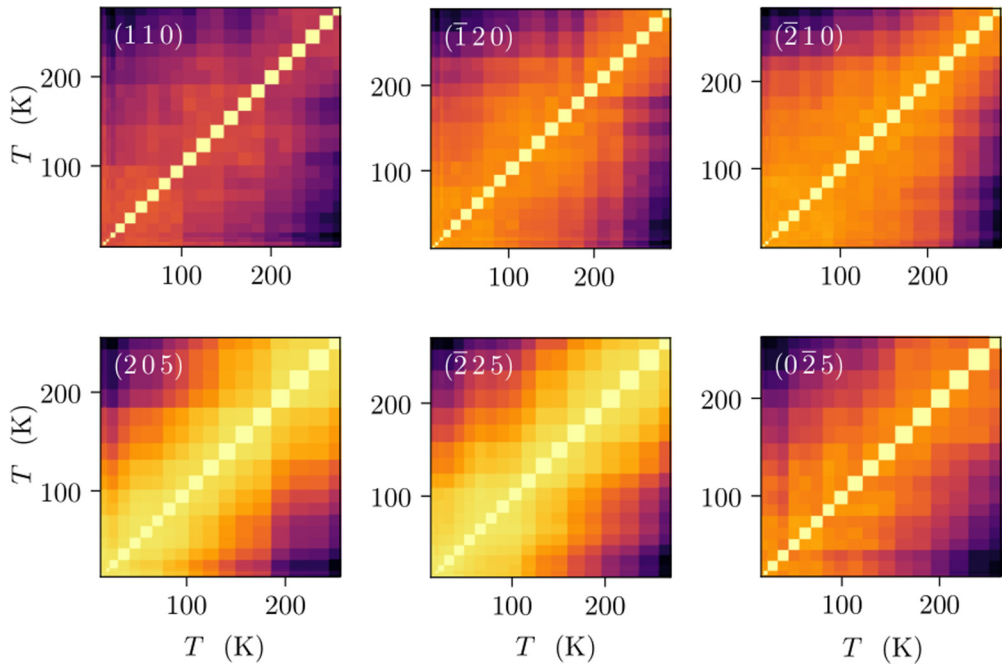

FIG. 6. Color maps of the correlation function of the Bragg scattering data taken at two sets of equivalent reflections; the correlation function is plotted against the two temperatures to be compared. For all reflections there is no indication of a discontinuity of the correlation function as is expected for a structural phase transition.

$U_{13} = U_{23} = 0$, and $U_{12} = 2U_{11}$. Therefore the refinement in space group $C2/m$ adds only four additional parameters (two positional parameters and two twin fractions). We can compare the reliability factors of the $C2/m$ refinements with those obtained in $R\bar{3}m$ by describing the high-symmetry phase in the low-symmetry setting. As can be seen in Table V in the Appendix, for the three refinements there is a significant improvement in all reliability factors that is also reflected in a reduction of the goodness-of-fit values. Note that the $R\bar{3}m$ and $C2/m$ refinements cannot be directly compared, because in the former case the data set is much smaller by merging many equivalent reflections. The structural parameters obtained in these refinements are given in Table III.

Further support for the symmetry reduction is given by the good agreement of the five different refinements. We always find a significant displacement of the Bi positions while the Se3 ion stays at the high-symmetry position as shown in Table III. The Bi displacement is illustrated in Fig. 5. The twin fractions indicate an almost equal occupation of the three twin orientations in the two large crystals studied here. Note, however, that the monoclinic distortion of the translation lattice is too small to be detected with the resolution of the single-crystal neutron diffraction experiment.

In spite of its weakness the structural distortion can be essential for the observation of a large anisotropy in the nematic superconducting state by poling the superconducting domains similar to the case of $Cu_{1.5}(PbSe)_5(Bi_2Se_3)_6$, where the nematic axis follows an intrinsic structural symmetry breaking [29]. The monoclinic distortion is the natural candidate to generate the uniaxial strain discussed by Venderbos *et al.* [30] to lift the degeneracy of the two superconducting components. The nematic superconducting transition exhibits an improper ferroelastic character and can thus be efficiently poled by small strain.

Evidence for a structural distortion was obtained also for Sr-doped Bi_2Se_3 by high-resolution x-ray experiments at room temperature [19] and by a tiny anomaly in the thermal expansion occurring slightly above the superconducting transition in a Nb-doped sample [31]. In both cases the structural distortion is well below the resolution in our experiments. But qualitatively the room-temperature distortion reported for the Sr system [19] corresponds to our finding of a monoclinic space group for Cu doping.

Further support for the reliability of these structural refinements can be obtained from the anisotropic displacement parameters given in Table VI in the Appendix. The small displacement of the Bi atom is visible in a minor reduction of the Bi U_{11} parameter in space group $C2/m$. In general there is a strong anisotropy of the displacement parameters with $U_{33} > U_{11}$, which can be explained by the layered character of the $Cu_xBi_2Se_3$ structure that exhibits strong bonding only within the quintuple layers. Therefore, c-polarized phonons must be much softer and imply large U_{33} values.

In the high-symmetry space group $R\bar{3}m$, there are two different Bi-Se distances: one from Bi to the Se atom at the border of the van der Waals gap and another one to the Se in the middle of the quintuple layer. These two distances amount to 2.8642(25) Å and 3.0745(23) Å, respectively. We use the c parameters obtained on our crystals, the in-plane lattice parameter from Ref. [17] and the structural parameters are averaged from refinements of the data collected at 1.9 K and 2 K. In the low-symmetry space group $C2/m$, each of these two distances splits into two different ones; see Fig. 5. The distance from the Bi atom to one of the the border Se atoms amounts to 2.8381(28) Å and the distances to the

other two Se atoms at the border are 2.8769(26) Å. The other distance splits into 3.0980(24) Å (occurring once) and two 3.0635(23) Å distances. Already in the high-symmetry phase the Bi ion is not situated at the center of the surrounding octahedron but moves toward the border of the quintuple layer. In Bi_2Se_3, Bi shows a formal 3+ valence state, which typically exhibits lone-pair behavior [32–34]. For Bi^{3+}, there is a pair of electrons outside the filled Xe shell, whose probability density can deviate from spherical symmetry. The strong off-centering in the high-symmetry structure can already be related with such an effect. The structural symmetry-breaking displacement in the low-symmetry phase $C2/m$ allows for horizontal off-centering of the lone-pair electron distribution.

If one admits a loss of inversion symmetry, the low-symmetry phase breaking the rotational axis without a loss of translation symmetry corresponds to space group Cm [28]. Note, however, that there is no evidence of broken inversion symmetry so far. Describing the structure in Cm requires 13 additional structural parameters and at least two twin parameters. We have refined this structural model with all 5 data sets, but we do not obtain evidence for such a distortion. The large number of additional parameters combined with the twinning impairs a reliable refinement.

IV. CONCLUSIONS

Our comprehensive neutron diffraction studies on superconducting single crystals of $Cu_xBi_2Se_3$ with $x \sim 0.3$ show that the dopant is not simply occupying the central intercalation position, but also at other proposed sites we do not detect significant amounts of Cu. The position of the Cu ion remains a mystery, but the enhanced thickness of the van der Waals gap supports the idea of intercalation between the layers. For any Cu incorporated in the Bi_2Se_3 structure, we assume considerable disorder arising from clustering to hide it in diffraction studies. We also do not find any evidence for a structural phase transition occurring between room temperature and the superconducting phase similar to caloric studies. However, the five collected Bragg reflection data sets consistently indicate a weak structural distortion lowering the symmetry to the monoclinic space group $C2/m$. This monoclinic distortion can be related to the lone electron pair of the Bi and be essential for the analysis of the nematic superconductivity in doped Bi_2Se_3 in spite of its weakness.

Single-crystal neutron diffraction data from the D9 diffractometer are available [35].

ACKNOWLEDGMENTS

This work was funded by the Deutsche Forschungsgemeinschaft (DFG, German Research Foundation), Project No. 277146847, CRC 1238, projects A02, A04, and B04.

APPENDIX A

1. Additional information about the refinements

In Table IV, we compare the reliability factors of refinements in space group $R\bar{3}m$ with empty, full, and partially occupied intercalation position at (0 0 1/2). We can exclude a significant Cu occupation of this site.

TABLE IV. Occupation of the intercalation position (0 0 1/2) by Cu in the refinements in space group $R\bar{3}m$; all reliability values are given in percent.

			Without Cu	With Cu	Free occ(Cu)
S1	1.9 K	R_{obs} (wR_{obs}):	3.07 (3.55)	12.99 (14.48)	3.07 (3.54)
		R_{all} (wR_{all}):	3.71 (3.71)	14.09 (14.61)	3.69 (3.70)
				occ(Cu):	−0.006(5)
	4.4 K	R_{obs} (wR_{obs}):	5.05 (5.25)	14.51 (16.25)	4.98 (5.24)
		R_{all} (wR_{all}):	5.71 (5.36)	15.36 (16.34)	5.74 (5.38)
				occ(Cu):	0.000(7)
	300 K	R_{obs} (wR_{obs}):	3.15 (4.83)	15.32 (17.29)	3.15 (4.83)
		R_{all} (wR_{all}):	4.69 (5.04)	16.92 (17.40)	4.69 (5.04)
				occ(Cu):	0.000(7)
S3	2 K	R_{obs} (wR_{obs}):	3.12 (3.97)	14.49 (18.97)	3.10 (3.96)
		R_{all} (wR_{all}):	3.24 (3.99)	14.78 (19.02)	3.21 (3.97)
				occ(Cu):	−0.006(5)
	300 K	R_{obs} (wR_{obs}):	4.56 (5.08)	14.87 (17.31)	4.54 (5.07)
		R_{all} (wR_{all}):	4.83 (5.11)	15.54 (17.35)	4.79 (5.10)
				occ(Cu):	−0.005(7)

Table V compares the reliability factors of the refinements in space groups $R\bar{3}m$ and $C2/m$. The column below $R\bar{3}m$ gives the standard values for the high-symmetry refinement, which, however, cannot be directly compared to those in space group $C2/m$ because data are differently merged. Therefore, we have also described the high-symmetry phase in space group $C2/m$ by restraining the two extra parameters and by setting fixed domain ratios. This can be directly compared to the refinements in $C2/m$ as indicated by the arrows. With the five data sets, we obtain a weak but significant reduction of the reliability parameters in agreement with improved goodness-of-fit values.

TABLE V. Refinements in space group $R\bar{3}m$ and $C2/m$ for different samples and temperatures. In order to compare the reliability values, the refinements in space group $C2/m$ were carried out with the same structural parameters as in $R\bar{3}m$ (left of the arrow "→") and then with the structural parameters refined according to space group $C2/m$ (right of the arrow "→"). The wR_{all} values improve by approximately 0.5%; all reliability values are given in percent.

		$R\bar{3}m$	$C2/m$
S1	1.9 K	R_{obs} (wR_{obs}) = 3.07 (3.55)	3.35 (3.69) → 3.07 (3.46)
		R_{all} (wR_{all}) = 3.71 (3.71)	4.82 (4.04) → 4.68 (3.62)
		GoF = 2.07	1.67 → 1.51
	4.4 K	R_{obs} (wR_{obs}) = 5.05 (5.25)	4.90 (5.33) → 4.78 (5.22)
		R_{all} (wR_{all}) = 5.71 (5.36)	6.57 (5.69) → 6.38 (5.36)
		GoF = 2.81	2.21 → 2.10
	300 K	R_{obs} (wR_{obs}) = 3.15 (4.83)	4.07 (5.29) → 3.97 (5.22)
		R_{all} (wR_{all}) = 4.69 (5.04)	6.32 (5.67) → 6.29 (5.47)
		GoF = 2.74	2.31 → 2.25
S3	2 K	R_{obs} (wR_{obs}) = 3.12 (3.97)	3.41 (3.99) → 2.96 (3.52)
		R_{all} (wR_{all}) = 3.24 (3.99)	4.14 (4.14) → 3.79 (3.60)
		GoF = 2.77	2.16 → 1.90
	300 K	R_{obs} (wR_{obs}) = 4.56 (5.08)	4.78 (5.43) → 4.24 (4.94)
		R_{all} (wR_{all}) = 4.83 (5.11)	5.83 (5.60) → 5.68 (5.03)
		GoF = 3.26	2.55 → 2.32

TABLE VI. Anisotropic displacement parameters (ADPs) of the atoms of Bi_2Se_3 of the samples S1 and S3 at different temperatures refined in space groups $R\bar{3}m$ and $C2/m$. The constraints for ADPs in space group $R\bar{3}m$, $U_{11} = U_{22} = 2U_{12}$ and $U_{13} = U_{23} = 0$, are also used in $C2/m$, and all parameters are given in 10^{-4} Å^2.

			$R\bar{3}m$		$C2/m$	
			U_{11}	U_{33}	U_{11}	U_{33}
S1	1.9 K	Bi1	42(4)	119(7)	25(3)	118(3)
		Se2	45(5)	100(10)	27(5)	112(5)
		Se3	39(4)	128(9)	43(4)	113(4)
	4.4 K	Bi1	97(5)	188(10)	76(4)	181(6)
		Se2	95(6)	188(13)	73(6)	192(9)
		Se3	99(5)	198(12)	97(5)	172(7)
	300 K	Bi1	155(7)	334(13)	141(5)	331(6)
		Se2	132(9)	255(15)	122(9)	259(9)
		Se3	147(8)	287(13)	147(8)	277(7)
S3	2 K	Bi1	13(4)	100(6)	14(2)	91(2)
		Se2	10(4)	73(8)	16(3)	68(3)
		Se3	16(4)	103(7)	21(2)	95(2)
	300 K	Bi1	83(7)	212(12)	78(4)	197(5)
		Se2	68(9)	120(15)	69(7)	117(7)
		Se3	77(8)	159(13)	85(5)	145(5)

The anisotropic displacement parameters obtained in the refinements of the $R\bar{3}m$ and $C2/m$ structures with the five data sets are shown in Table VI. In both structures, we keep the symmetry constraints of the rhombohedral structure. The displacement parameters are quite anisotropic with larger U_{33} values, which reflects the layered character of the Bi_2Se_3 crystal structure. Strong bonds only exist within the quintuples layers, while the interlayer bonding only arises from the van der Waals potential. The refinements indicate soft c-polarized phonons.

2. Analysis of the resemblance of Bragg scattering data

We have analyzed the resemblance of Bragg scattering data taken as function of temperature by calculating the correlation function for data taken at temperatures T_1 and T_2 [36]:

$$r(T_1, T_2) = \frac{\overline{I_{T_1} I_{T_2}} - \overline{I_{T_1}}\,\overline{I_{T_2}}}{\sqrt{\left(\overline{I_{T_1}^2} - \overline{I_{T_1}}^2\right)\left(\overline{I_{T_2}^2} - \overline{I_{T_2}}^2\right)}}, \tag{A1}$$

where I_T is the number of counts at temperature T and the vinculum denotes the mean with respect to all pixels and ω positions.

The correlation function defined in Eq. (A1) does not depend on the total intensity of the signal, but only on the distribution along the ω scan and the pixels. If the peak shapes or positions differ at two temperatures T_1 and T_2, the quantity $r(T_1, T_2)$ is small.

In Fig. 6 we show color maps of the $r(T_1, T_2)$ values plotted against the two temperatures. It can be seen that there is a strong tendency that the detector images are similar for similar temperatures and differ more strongly if the temperature difference is greater. If the detector images changed suddenly, there would be two temperature intervals, where correlation coefficients are high for temperatures that lie in the same interval and lower for temperatures in different intervals. We conclude that also the shape and position of the reflections show no indication for a structural phase transition.

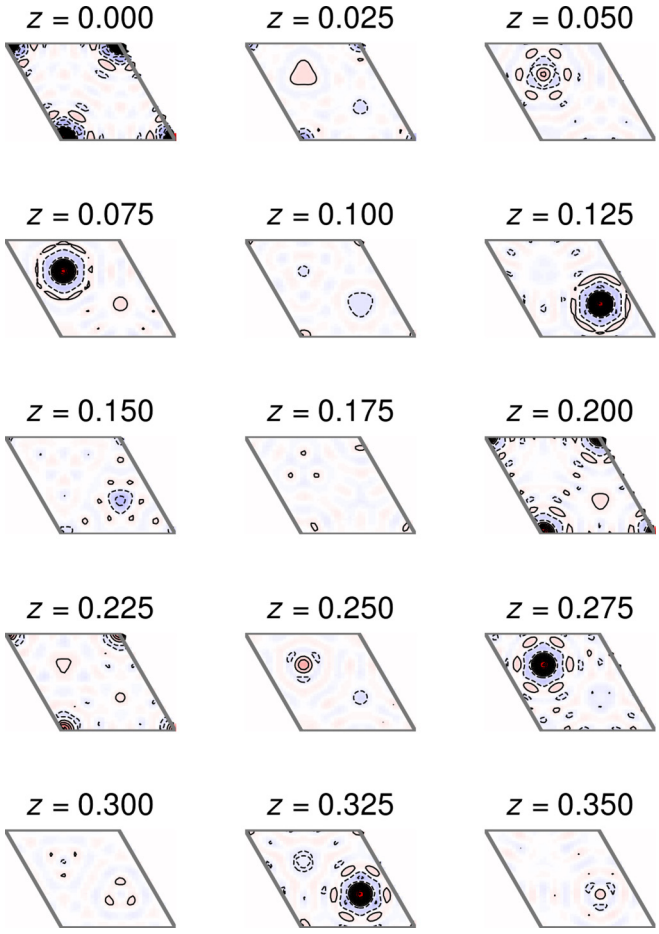

FIG. 7. Total scattering maps calculated with data set taken on sample S1 at 1.9 K. The Bi and Se atoms are clearly visible, but there is no evidence of any extra scattering in these maps.

3. Calculated scattering density maps

Extra scattering arising from the inserted atoms can be visualized in the scattering maps obtained by Fourier transformation. Such calculated maps are shown in Fig. 7 for Bragg reflection data taken with sample S1 at 1.9 K. However, there is no evidence for extra scattering in these maps, which only show the expected peaks at the Bi and Se positions. Fourier maps calculated for the other sample S3 at 2 K also do not indicate extra scattering.

[1] Y. S. Hor, A. J. Williams, J. G. Checkelsky, P. Roushan, J. Seo, Q. Xu, H. W. Zandbergen, A. Yazdani, N. P. Ong, and R. J. Cava, Phys. Rev. Lett. **104**, 057001 (2010).

[2] L. Fu and E. Berg, Phys. Rev. Lett. **105**, 097001 (2010).

[3] Z. Liu, X. Yao, J. Shao, M. Zuo, L. Pi, S. Tan, C. Zhang, and Y. Zhang, J. Am. Chem. Soc. **137**, 10512 (2015).

[4] Shruti, V. K. Maurya, P. Neha, P. Srivastava, and S. Patnaik, Phys. Rev. B **92**, 020506(R) (2015).
[5] Y. Qiu, K. N. Sanders, J. Dai, J. E. Medvedeva, W. Wu, P. Ghaemi, T. Vojta, and Y. S. Hor, arXiv:1512.03519.
[6] K. Matano, M. Kriener, K. Segawa, Y. Ando, and G. Zheng, Nat. Phys. **12**, 852 (2016).
[7] S. Yonezawa, Condens. Matter **4**, 2 (2018).
[8] S. Yonezawa, K. Tajiri, S. Nakata, Y. Nagai, Z. Wang, K. Segawa, Y. Ando, and Y. Maeno, Nat. Phys. **13**, 123 (2017).
[9] T. Asaba, B. J. Lawson, C. Tinsman, L. Chen, P. Corbae, G. Li, Y. Qiu, Y. S. Hor, L. Fu, and L. Li, Phys. Rev. X **7**, 011009 (2017).
[10] Y. Pan, A. M. Nikitin, G. K. Araizi, Y. K. Huang, Y. Matsushita, T. Naka, and A. de Visser, Sci. Rep. **6**, 28632 (2016).
[11] G. Du, Y. Li, J. Schneeloch, R. D. Zhong, G. Gu, H. Yang, H. Lin, and H.-H. Wen, Science China Physics, Mechanics & Astronomy **60**, 037411 (2017).
[12] J. Shen, W.-Y. He, N. F. Q. Yuan, Z. Huang, C.-w. Cho, S. H. Lee, Y. S. Hor, K. T. Law, and R. Lortz, npj Quantum Mater. **2**, 59 (2017).
[13] M. P. Smylie, K. Willa, H. Claus, A. E. Koshelev, K. W. Song, W.-K. Kwok, Z. Islam, G. D. Gu, J. A. Schneeloch, R. D. Zhong, and U. Welp, Sci. Rep. **8**, 7666 (2018).
[14] Y.-L. Wang, Y. Xu, Y.-P. Jiang, J.-W. Liu, C.-Z. Chang, M. Chen, Z. Li, C.-L. Song, L.-L. Wang, K. He, X. Chen, W.-H. Duan, Q.-K. Xue, and X.-C. Ma, Phys. Rev. B **84**, 075335 (2011).
[15] M. Kriener, K. Segawa, Z. Ren, S. Sasaki, and Y. Ando, Phys. Rev. Lett. **106**, 127004 (2011).
[16] M. Kriener, K. Segawa, Z. Ren, S. Sasaki, S. Wada, S. Kuwabata, and Y. Ando, Phys. Rev. B **84**, 054513 (2011).
[17] S. Nakajima, J. Phys. Chem. Solids **24**, 479 (1963).
[18] Z. Li, M. Wang, D. Zhang, N. Feng, W. Jiang, C. Han, W. Chen, M. Ye, C. Gao, J. Jia, J. Li, S. Qiao, D. Qian, B. Xu, H. Tian, and B. Gao, Phys. Rev. Mater. **2**, 014201 (2018).
[19] A. Y. Kuntsevich, M. A. Bryzgalov, V. A. Prudkoglyad, V. P. Martovitskii, Y. G. Selivanov, and E. G. Chizhevskii, New J. Phys. **20**, 103022 (2018).
[20] D9: Hot Neutron Four-Circle Diffractometer, Institut Laue-Langevin, 71 avenue des Martyrs CS 20156, 38042 Grenoble Cedex 9, France.
[21] A. Albinati *et al.*, in *International Tables for Crystallography*, Vol. C, edited by E. Prince (Kluwer Academic Publishers, Dordrecht/Boston/London, 2004).
[22] C. Pérez Vicente, J. L. Tirado, K. Adouby, J. C. Jumas, A. A. Touré, and G. Kra, Inorg. Chem. **38**, 2131 (1999).
[23] K. Sobczak, P. Strak, P. Kempisty, A. Wolos, A. Hruban, A. Materna, and J. Borysiuk, Phys. Rev. Mater. **2**, 044203 (2018).
[24] V. Petříček, M. Dušek, and L. Palatinus, Z. Kristallogr. **229**, 345 (2014).
[25] In order to calculate the mean Cu occupation we add the contributions from the Cu sites (i) to (iv) and average over the five data sets.
[26] H. Arnold, in *International Tables for Crystallography*, Vol. A, edited by T. Hahn (Kluwer, Dordrecht/Boston/London, 2002).
[27] K. Willa, R. Willa, Kok Wee Song, G. D. Gu, J. A. Schneeloch, R. Zhong, A. E. Koshelev, Wai-Kwong Kwok, and U. Welp, Phys. Rev. B **98**, 184509 (2018).
[28] H. T. Stokes and D. M. Hatch, *Isotropy Subgroups of the 230 Crystallographic Space Groups* (World Scientific, Singapore, 1988).
[29] L. Andersen, Z. Wang, T. Lorenz, and Y. Ando, Phys. Rev. B **98**, 220512(R) (2018).
[30] J. W. F. Venderbos, V. Kozii, and Liang Fu, Phys. Rev. B **94**, 094522 (2016).
[31] Chang-woo Cho, Junying Shen, Jian Lyu, S. H. Lee, Yew San Hor, M. Hecker, J. Schmalian, and R. Lortz, arXiv:1905.01702.
[32] L. E. Orgel, J. Chem. Soc., 3815 (1959).
[33] J. Galy and G. Meunier, J. Solid State Chem. **13**, 142 (1975).
[34] A. Laarif and F. Theobald, Solid State Ionics **21**, 183 (1986).
[35] Data are available at https://doi.ill.fr/10.5291/ILL-DATA.5-41-914 and https://doi.ill.fr/10.5291/ILL-DATA.5-11-426.
[36] O. Bikondoa, J. Appl. Crystallogr. **50**, 357 (2017).